Supplementary Information for:

Self-stratified Photonic Radiative Cooling Composites with Asymmetric Thermal Conductivity

Yi Zhou,[1] Canhui Lu,[1] Wanlin Wu,[1] Rui Xiong[1*]

1. State Key Laboratory of Polymer Materials Engineering, Polymer Research Institute of Sichuan University, Chengdu, 610065 China

*Corresponding authors. rui.xiong@scu.edu.cn (R. X.).

Supporting Discussions

Note S1. Average solar reflectance and average infrared emissivity of atmospheric transparent windows[1]

The spectrally-averaged solar reflectance, $\bar{R}_{solar}$, can be evaluated using the spectral solar radiation intensity of air mass 1.5 ($I_{solar}(\lambda)$, AM1.5) as a weighting factor, as given by,

$$\bar{R}_{solar} = \frac{\int I_{solar}(\lambda) R_{solar}(\lambda) d\lambda}{\int I_{solar}(\lambda) d\lambda} \quad \text{(S1)}$$

where $R_{solar}(\lambda)$ is spectral reflectance in solar region.

The spectrally-averaged absorption efficiency, $\bar{\varepsilon}$, can be evaluated using the spectral blackbody emissive power in the 8–13 μm range as a weighting factor. This is given by,

$$\bar{\varepsilon} = \frac{\int_{8\mu m}^{13\mu m} E_b(\lambda,T)\varepsilon(\lambda) d\lambda}{\int_{8\mu m}^{13\mu m} E_b(\lambda,T) d\lambda} \quad \text{(S2)}$$

where, $\varepsilon(\lambda)$ is spectral emissivity in the 8-13 μm range, $E_b(\lambda,T) = \frac{2hc_0^2}{\lambda^5\left[\exp\left(\frac{hc_0}{\lambda k_b T}\right) - 1\right]}$ is black body emissivity, h=6.626×10^{-34} J·s is the universal Plank constant, k_b =1.381 × 10^{-23}J/K is the Boltzmann constant, and c_0 = 2.998 × 10^8 m/s is the speed of light in vacuum.

Note S2. Radiative cooling power estimation[2–4]

The net cooling power ($P_{cooling}$) of the sample can be estimated from

$$P_{cooling} = P_{rad} - P_{sun} - P_{amb} - P_{con} \quad \text{(S3)}$$

where,

P_{rad} is the power density of thermal radiation emitted by the samples,

P_{sun} is the heating power density of solar irradiation,

P_{amb} is the power density of downward thermal radiation from the atmosphere,

P_{conv} is the effective power density loss including convection and conduction from the samples,

P_{rad} can be derived from the measured emittance spectrum of the sample by,

$$P_{rad} = \int_{\lambda_1}^{\lambda_2} \varepsilon(\lambda) E_b(\lambda,T) d\lambda \quad \text{(S4)}$$

where $\varepsilon(\lambda)$ is the sample emittance and $E_b(\lambda,T)$ is blackbody radiation intensity as a function of emitter temperature according to Planck's law.

P_{sun} from solar irradiation is calculated by integrating sample emittance over the Air Mass 1.5 (AM1.5) solar spectrum as,

$$P_{sun} = \int_{0.25\mu m}^{2.5\mu m} (1 - R_{solar}(\lambda)) I_{solar}(\lambda) d\lambda \quad \text{(S5)}$$

P_{amb} is the amount of power emitted from the atmosphere and absorbed by the sample. The

emittance spectra of the atmosphere and the cellulose sample are used.

$$P_{amb} = \int_{0}^{\frac{\Pi}{2}} \int_{2.5\mu m}^{25\mu m} \varepsilon(\lambda)\varepsilon_{amb}(\lambda,\theta)E_b(\lambda,T_{amb})d\lambda cos\theta d\theta \quad \text{(S6)}$$

where the angular part of the atmospheric emittance can be obtained by $\varepsilon_{amb}(\lambda,\theta) = 1 - \tau^{1/COS\theta}$, where τ is the angular atmospheric transmittance.

The P_{con} can be evaluated via the sample temperature T, ambient temperature T_{amb}, and the effective heat transfer coefficient h_{con} as,

$$P_{con} = h_{con}(T_{amb} - T) \quad \text{(S7)}$$

Here, we evaluate and compare the isothermal theoretical cooling power of the samples assuming the same temperature for the sample and the ambient such that the convection loss term can be neglected.

Supporting Figures

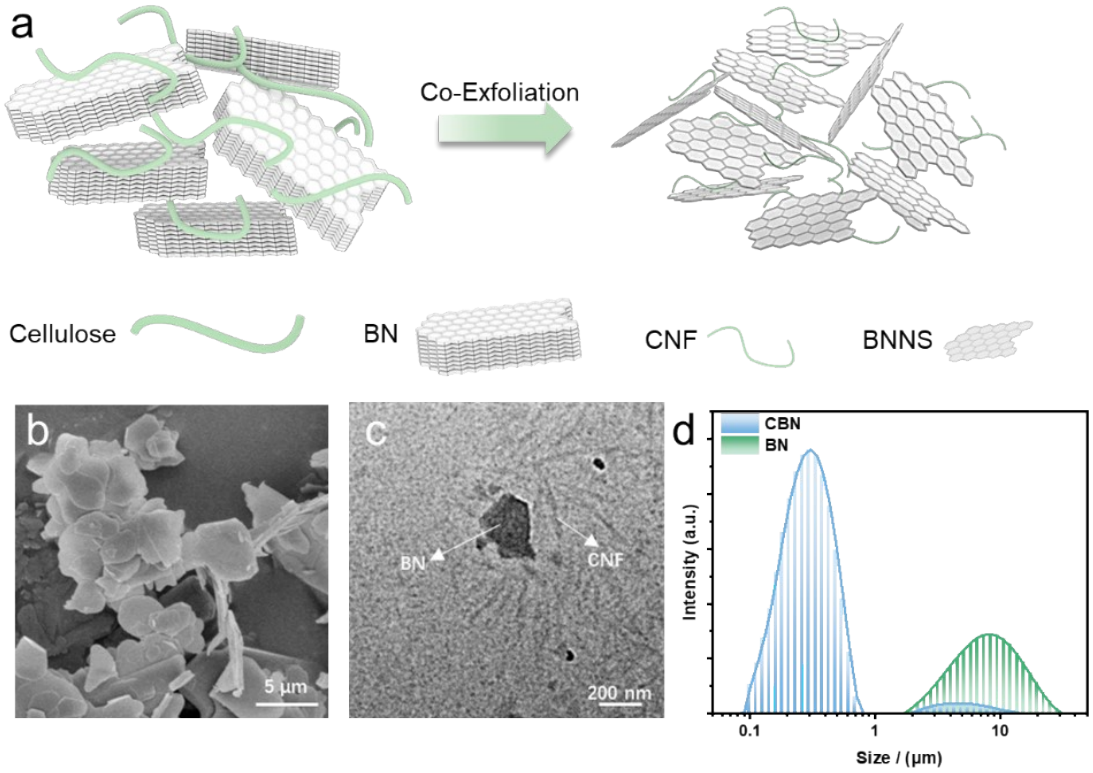

Fig. S1. (a) Schematic diagram of the co-exfoliation of BN and cellulose. (b) SEM image of BN before co-exfoliation. (c) TEM image of CBN suspension. (d) DLS of BN and CBN suspension.

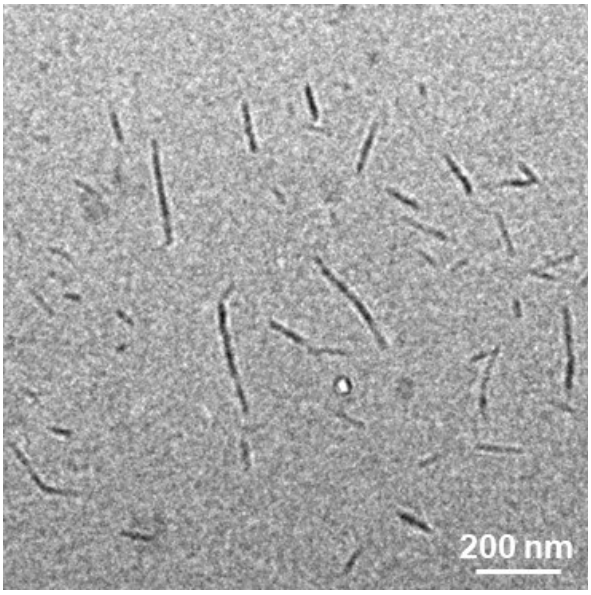

Fig. S2. TEM image of CNC suspension.

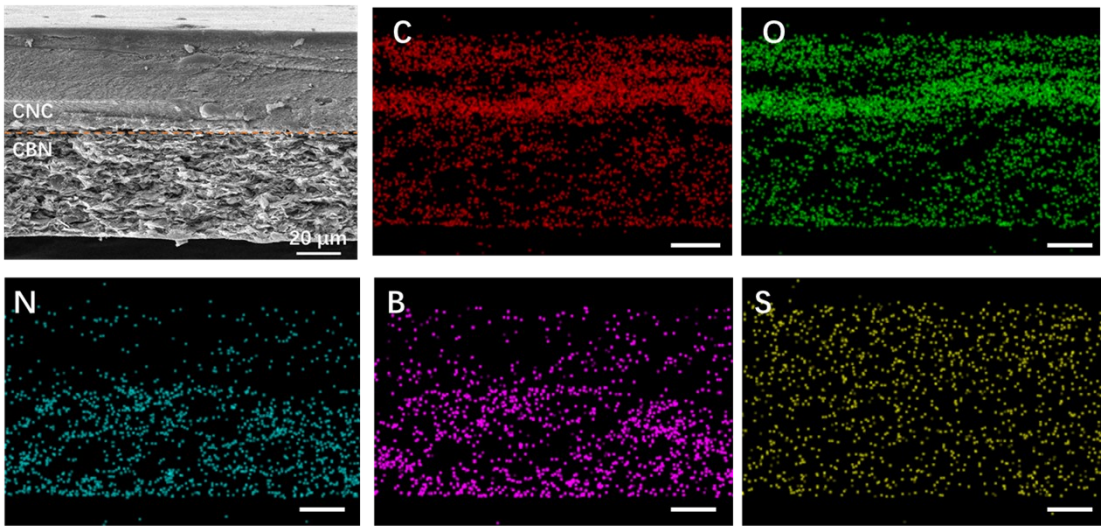

Fig. S3. Cross section EDX elemental analysis of the CBN/CNC.

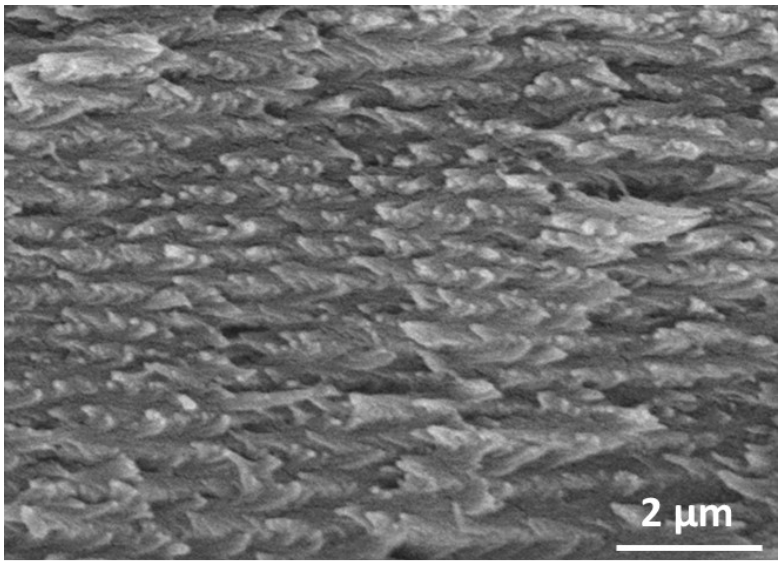

Fig. S4. SEM image of CNC-rich layer.

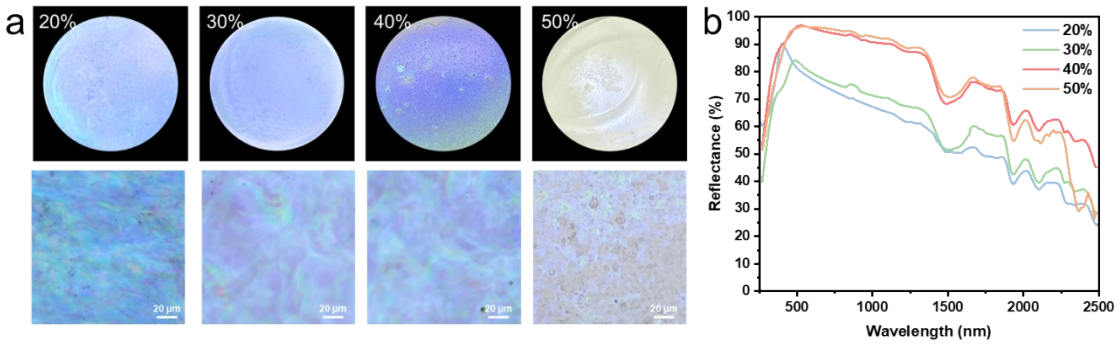

Fig. S5. (a) Photographs and POM images of CBN/CNC with different CBN mass production. (b) Reflectance spectra of CBN/CNC with different CBN mass production.

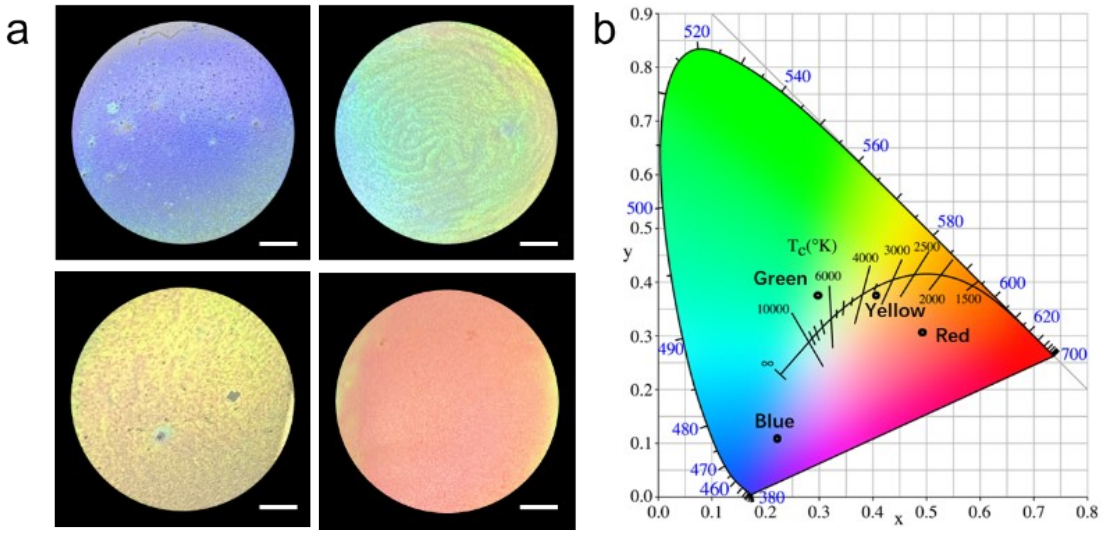

Fig. S6. Photographs (a) and CIE chromaticity coordinates (b) of CBN/CNC with different colors (Scale bar = 1 cm).

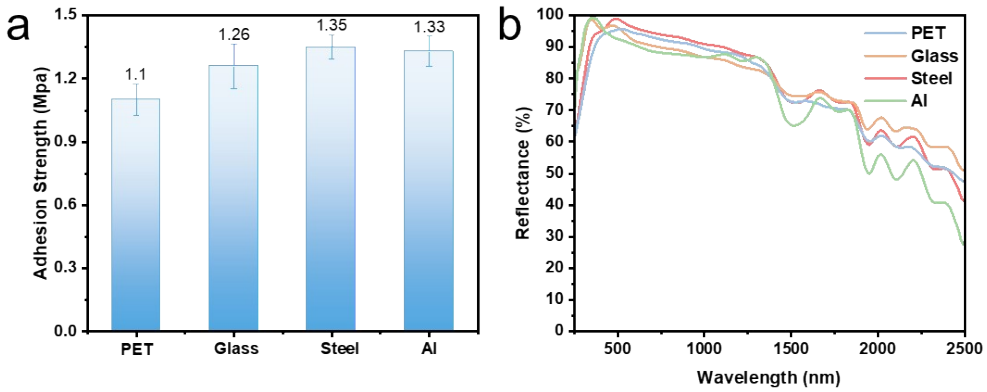

Fig. S7. The adhesion strength (a) and reflectance spectra (b) of CBN/CNC on different substrates.

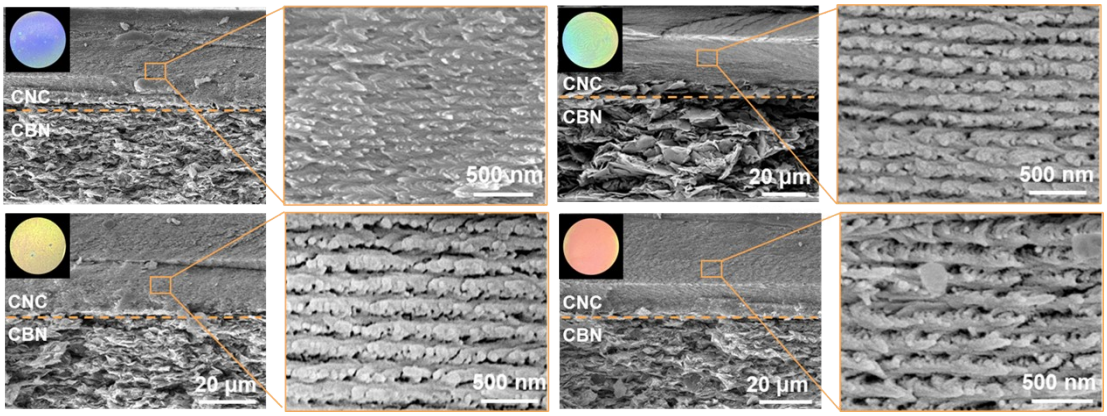

Fig. S8. Cross section SEM images of CBN/CNC with different colors.

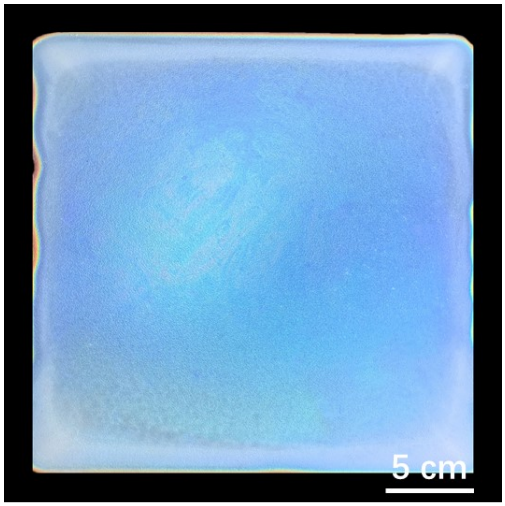

Fig. S9. Photograph of large-scale CBN/CNC.

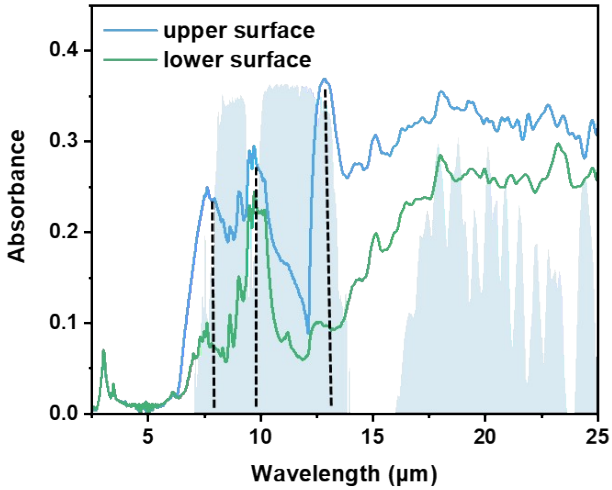

Fig. S10. FTIR spectrums of CBN/CNC.

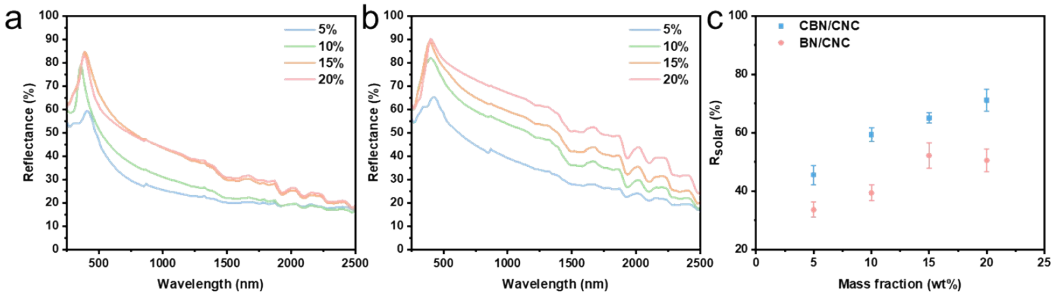

Fig. S11. Reflectance spectrums of BN/CNC (a) and CBN/CNC (b) with different BN (or CBN) loading. The average reflectance of BN/CNC and CBN/CNC across the solar spectrum.

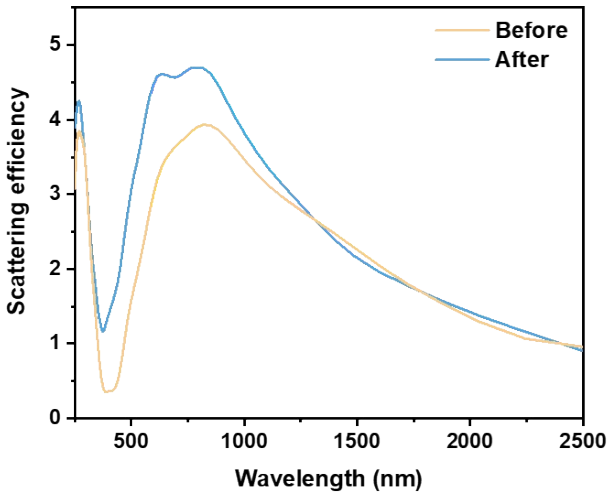

Fig. S12. Scattering efficiency of BN before and after co-exfoliated with cellulose.

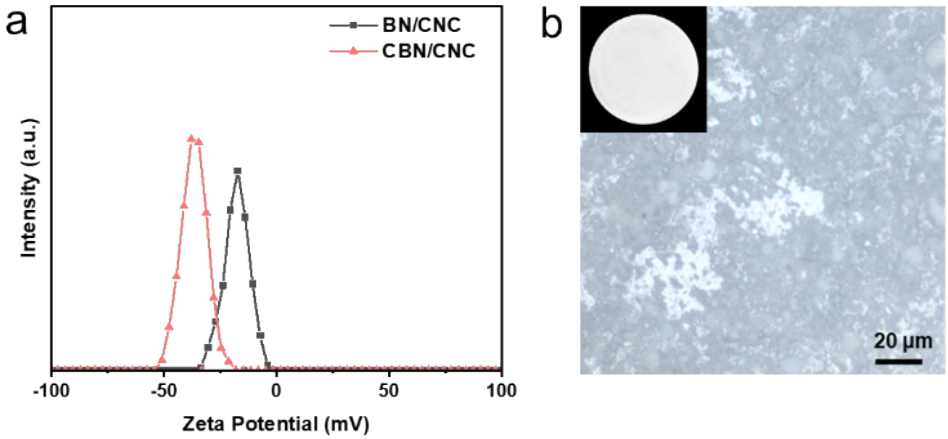

Fig. S13. (a) The zeta potential of BN/CNC and CBN/CNC. (b) Photograph and POM image of BN/CNC with a 30wt% BN loading.

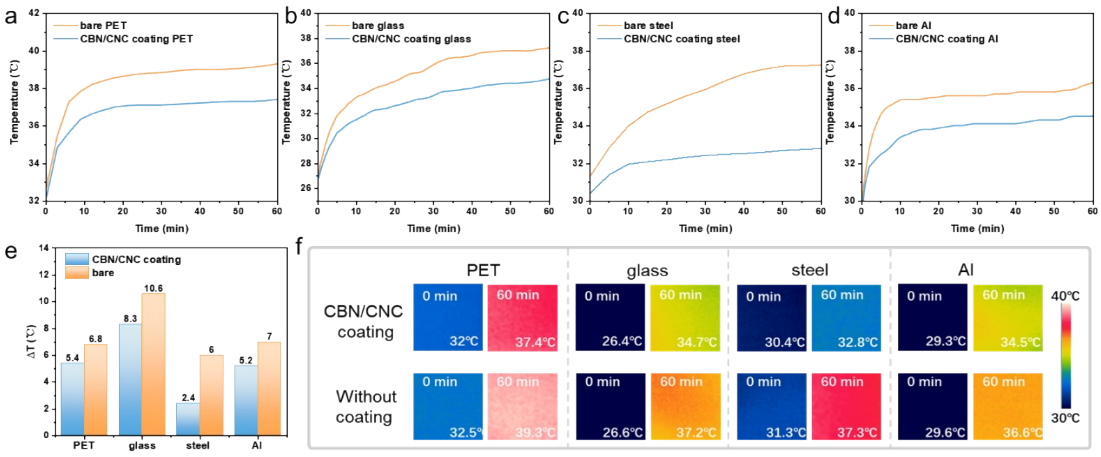

Fig. S14. Temperature variations over time of CBN/CNC coating PET (a), glass (b), steel (c) and Al (d). Temperature change tracking (e) and thermal infrared images (f) of CBN/CNC coated

substrates and bare substrates.

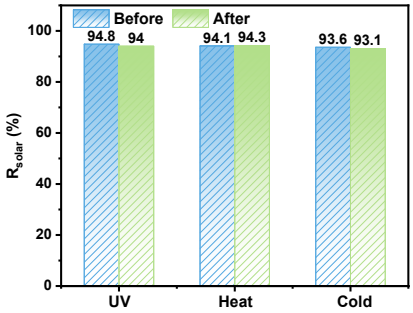

Fig. S15. Reflectance stability of CBN/CNC resistance to UV and high/low temperature

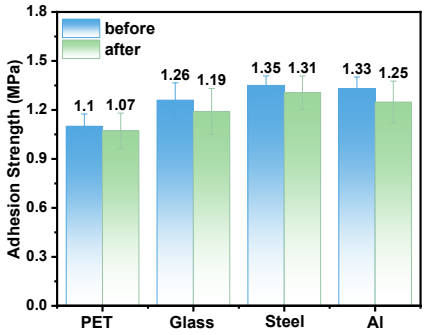

Fig. S16. The adhesion strength of CBN/CNC on different substrates before and after extreme environment testing.

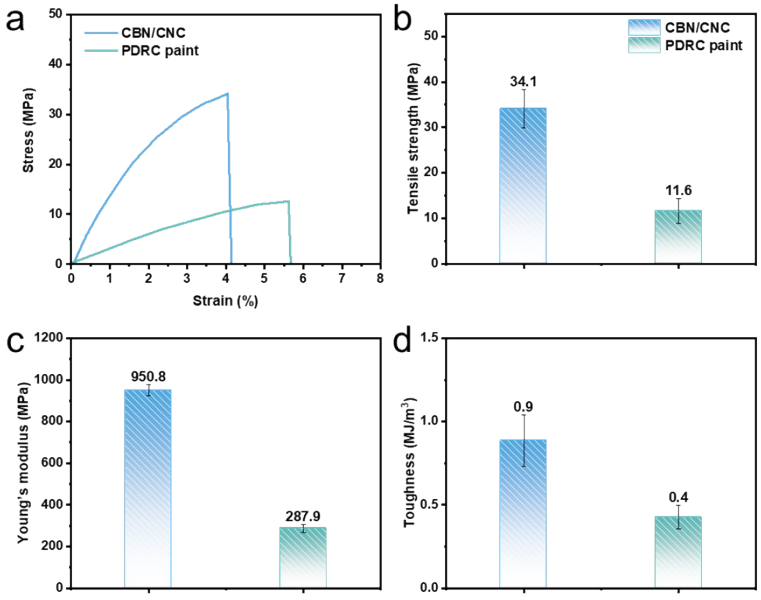

Fig. S17. Stress–strain curves (a) and strength (b), modulus (c), and toughness (d) of CBN/CNC and PDRC paint.

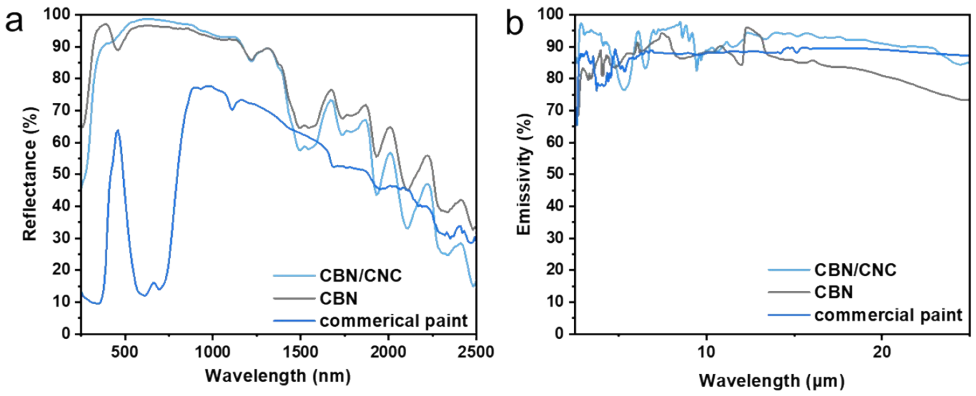

Fig. S18. Reflectance spectra (a) and thermal emissivity spectra (b) of CBN, CBN/CNC, and commercial paint.

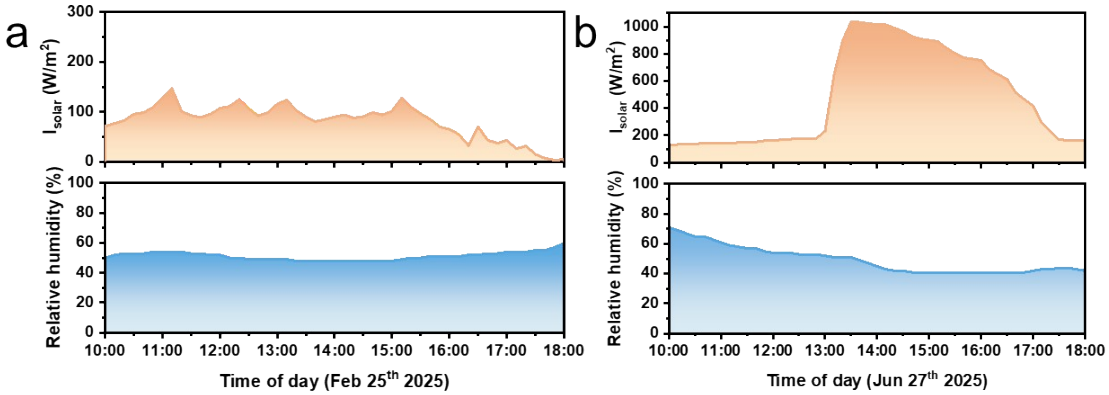

Fig. S19. Detailed recordings of solar irradiance and relative humidity during the outdoor testing period in the winter (a) and summer (b).

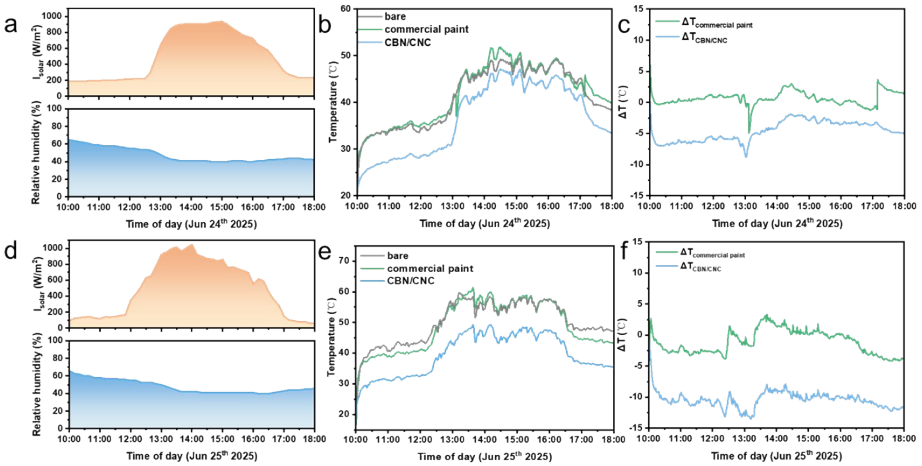

Fig. S20. Detailed recordings of solar irradiance and relative humidity during the outdoor testing period with the heat flux of 500 W/m^2 (a) and 1500 W/m^2 (d). Temperature recordings of bare equipment, commercial paint coating and CBN/CNC coating with the heat flux of 500 W/m^2 (b) and 1500 W/m^2 (e). Temperature below the bare equipment for commercial paint coating and CBN/CNC coating with the heat flux of 500 W/m^2 (c) and 1500 W/m^2 (f).

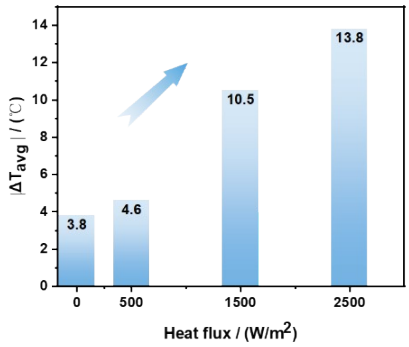

Fig. S21. The average ΔT between CBN/CNC coating box and bare box with different heat flux.

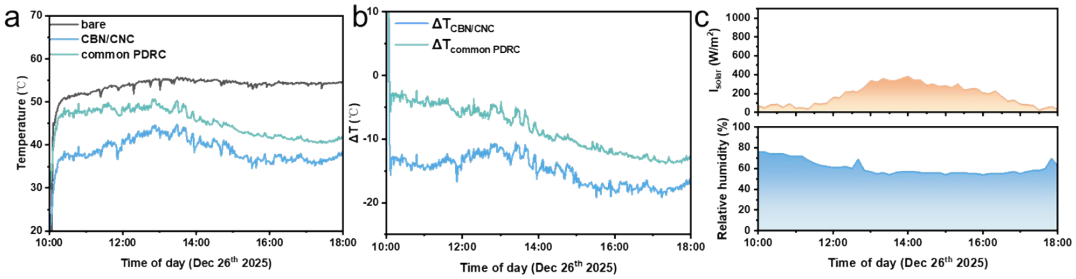

Fig. S22. (a) Temperature recordings of bare equipment, CBN/CNC coating and common PDRC coating. (b) Temperature below the bare equipment for CBN/CNC coating and common PDRC coating. (c) Detailed recordings of solar irradiance and relative humidity during the outdoor testing period.

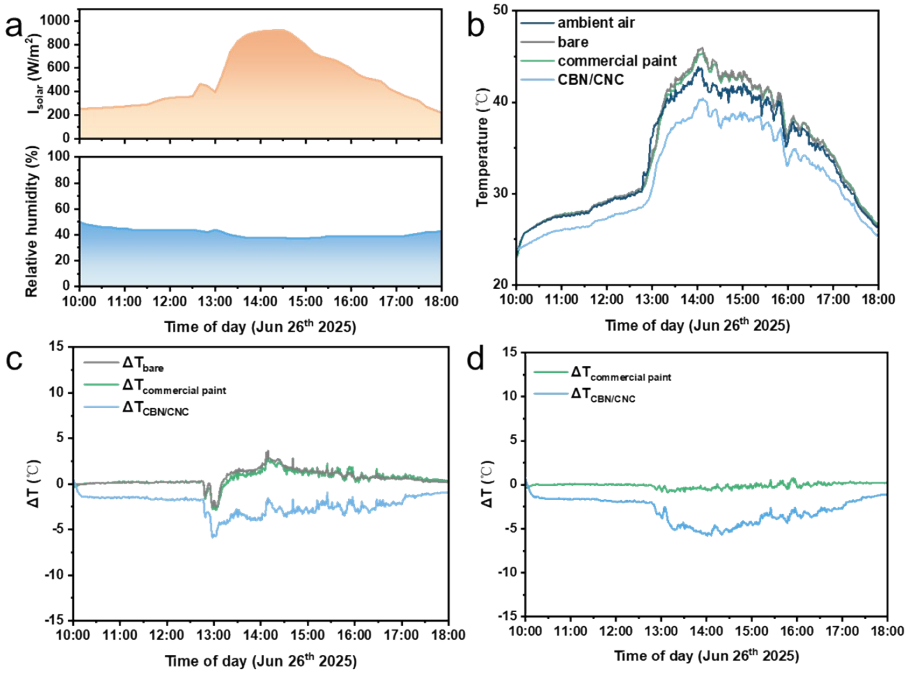

Fig. S23. (a) Detailed recordings of solar irradiance and relative humidity during the outdoor testing

period with the heat flux of 0 W/m^2. (b) Temperature recordings of bare equipment, commercial paint coating, CBN/CNC coating and ambient air with the heat flux of 0 W/m^2. Temperature below the ambient air (c) and bare equipment (d) for commercial paint coating and CBN/CNC coating.

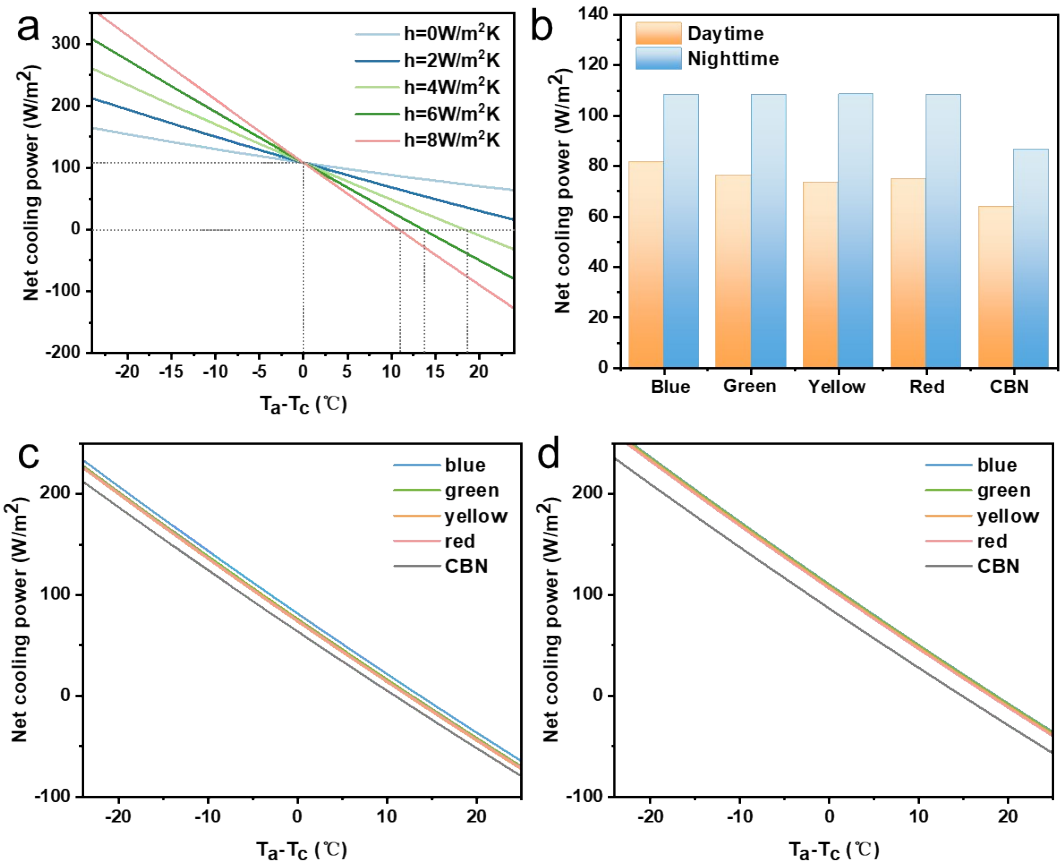

Fig. S24. (a) Calculated net cooling power of blue CBN/CNC at nighttime, with different h values. (b) Calculated net cooling power of CBN/CNC with different colors and CBN. Calculated net cooling power of CBN/CNC with different colors and CBN at daytime (c) and nighttime (d), with the h=0 W/m²·K.

Table S1. Above- and sub-ambient cooling performance of thermal radiation cooling solutions.

Materials	Above-Ambient Radiative Cooling			Sub-ambient Radiative Cooling		Reference
	I_{solar}/ W/m^2	Heat flux/ W/m^2	ΔT_{max}/°C	I_{solar}/W/m^2	ΔT_{max}/°C	
hBN/PDMS	800	700	3.9	700	4	5
		2000	14.3			
hBN/PVA	643.9	3000	13.49	-	-	6
SiO_2-BNNS	800	-	8	-	-	7
BN-PFA	>900	2000	8	800	~5	8
		3600	15-25 (compared with polymer)			
		8000	30 (compared with PFA)			
ANF/BN/Si	836.4	-	13.98	927.65	10.82	9

O_2/ graphene						
BN/Al_2O_3/PDMS	685	150	13.7	650	10.8	[10]
hBN/PVDF	-	-	11	950	7	[11]
BN/CNF/MTMS	-	700	9.1	800	3.3	[12]
LNS/HEMA	~900	-	2.1	~900	2.4	[13]
BN/TiO_2/PS-AA	800	4V	8 (compared with polymer)	800	5-8 (compared with polymer)	[14]
ANF/BNNS	1000	LED chip	17.2	1000	＞10	[15]
CBN/CNC	900	500	8.8	900	6.8	This work
	900	1500	13.5			
	>950	2500	17.8			

References

1 W. Zhu, B. Droguet, Q. Shen, Y. Zhang, T. G. Parton, X. Shan, R. M. Parker and T. Li, *Adv. Sci.*, 2022, **9**, 2202061.

2 T. Li, Y. Zhai, S. He, W. Gan, Z. Wei, M. Heidarinejad, D. Dalgo, R. Mi, X. Zhao, J. Song, J. Dai, C. Chen, A. Aili, A. Vellore, A. Martini, R. Yang, J. Srebric, X. Yin and L. Hu, *Science*, 2019, **364**, 760–763.

3 K. Bu, X. Huang, X. Li and H. Bao, *Adv Funct Materials*, 2023, **33**, 2307191.

4 X. Xue, M. Qiu, Y. Li, Q. M. Zhang, S. Li, Z. Yang, C. Feng, W. Zhang, J. Dai, D. Lei, W. Jin, L. Xu, T. Zhang, J. Qin, H. Wang and S. Fan, *Advanced Materials*, 2020, **32**, 1906751.

5 P. Li, A. Wang, J. Fan, Q. Kang, P. Jiang, H. Bao and X. Huang, *Adv Funct Materials*, 2022, **32**, 2109542.

6 Z. Wang, T. Wang, Q. Zhu, Z. Ding, M. Gu and Y. Zhang, *Adv Funct Materials*, 2025, **35**, 2501646.

7 B. Zhu, Y. Qin, M. Li, Z. Zhang, Y. Wang, R. Yang, K. Xu, J. Zhang, Y. Zhou, Y. Guo, X. Wang, Z. Wu, T. Cai, K. Nishimura, C.-T. Lin, Y. Li, N. Jiang, L. Li and J. Yu, *Nano Energy*, 2025, **141**, 111124.

8 T. Zhou, Z. Shao, Z. Sun, Y. Li, Q. Zhang, K. Li, C. Hou and H. Wang, *Adv Funct Materials*, 2025, e09358.

9 X. Yan, J. Liu, L. Zhang, Y. Zhong, B. Ji, W. Wu, B. Wang, X. Feng, L. Rong, H. Xu and Z. Mao, *Chemical Engineering Journal*, 2025, **523**, 168743.

10 X. Yu, X. Sun, A. Wang, C. Yang, Z. Wang and X. Wang, *ACS Appl. Mater. Interfaces*, 2025, **17**, 41124–41133.

11 H. Fu, Y. Zhang, X. Liu, H. Han, H. Kondo and H. Zhou, *Solar Energy Materials and Solar Cells*, 2024, **266**, 112660.

12 F. Xu, T. Zhu, Y. Wang, B. Ji, Y. Zhao, Y. Miao and C. Zhang, *Small*, 2025, **21**, 2503789.

13 Y. Wang, S. Liu, X. Zhang, Y. Liu, T. Zhu, B. Ji, J. Chen, Y. Cheng, W. Fan, Y.-E. Miao, N. Willenbacher, C. Zhang and T. Liu, *ACS Nano*, 2025, **19**, 19328–19339.

14 R. Ding, S. Feng, Z. Wu, F. Fan, H. Tang, C. Guo, Q. Chen, D. Kong and D. Zhao, *Nano Energy*, 2025, **146**, 111524.

15 G. Han, H. Cheng, Y. Feng, S. Zhang, J. Dong, B. Zhou, X. Liu, C. Liu, G. Tao and C. Shen, *Nat Commun*, 2025, **16**, 10533.